

EFFECT OF FOUNDATION SURFACE ROUGHNESS ON ULTIMATE BEARING CAPACITY OF AN ECCENTRICALLY LOADED FOUNDATION

Pham Ngoc Vinh, Pham Ngoc Quang*, Hoang Thang

The University of Danang - University of Science and Technology, Danang, Vietnam

*Corresponding author: pnquang@dut.udn.vn

(Received: November 01, 2023; Revised: December 02, 2023; Accepted: December 06, 2023)

Abstract - The study extensively investigated the ultimate bearing capacity (UBC) of an eccentrically loaded foundation under two scenarios (horizontal sandy soil and sandy soil slope), utilizing the Rigid Plastic Finite Element Method (RPFEM). To precisely simulate a diverse range of frictional conditions on the foundation surface roughness, a novel joint element is introduced, capable of accommodating both perfectly rough and perfectly smooth foundations. A novel constitutive equation is presented to model these joint elements, significantly influencing the failure mechanism of the shallow foundation. The study also examines the impact of the friction strength ϕ on the normalized vertical load V/V_{ult} . The RPFEM results reveal that the friction strength ϕ substantially influences the V/V_{ult} ratio for sandy soil slopes, while its effect is found to be negligible for horizontal sandy soil.

Key words - Ultimate bearing capacity; Shallow foundation; Sandy soil; Foundation roughness; Eccentric load; RPFEM

1. Introduction

In geotechnical engineering, shallow foundations are designed to withstand complex loading conditions resulting from a combination of vertical, horizontal, and moment loads. In practical applications, shallow foundations often face challenges when subjected to eccentric vertical loads. Meyerhof [1] addressed this issue for sand and clay by investigating the impact of eccentric loads on the ultimate bearing capacity (UBC) of shallow foundations. Meyerhof introduced the concept of effective width, denoted as $B'=B-2e$, where e represents the eccentricity length, indicating the distance from the loading point to the center of the shallow foundation. The use of effective width B' is common in foundation design to account for eccentric loading. Various studies, such as those by [2 - 5] have further investigated the influence of eccentric loads on the UBC through numerical analyses and model testing. Although many works, a comprehensive understanding of the UBC and the failure modes of shallow foundations remains elusive due to the limited scope of conditions considered in previous research, particularly concerning variations in foundation surface roughness. Therefore, a comprehensive understanding of the UBC and the failure mechanisms associated with eccentrically loaded shallow foundation is yet to be established, emphasizing the need for further research encompassing a broader range of conditions, including different levels of foundation surface roughness.

The objective of this study is to employ a self-developed RPFEM code for determining the ultimate bearing capacity (UBC) of an eccentrically loaded foundation on horizontal sandy soil and a sandy soil slope.

The investigation takes into account the influence of foundation surface roughness on the UBC. RPFEM, a technique previously applied in geotechnical engineering by [6 - 11], is utilized. Addressing challenges faced in prior studies, [4, 5, 12, 13, 14] introduced the concept of using an interface element to calculate the UBC and failure modes of shallow foundations. Their research emphasized the effectiveness of employing an interface element in these determinations. In this present study, the incorporation of new joint elements is extensive, examining failure mechanisms under both rough and smooth foundations. Two novel constitutive equations are introduced: the first relates to the material characteristics of the shallow foundation and the sandy soil, while the second addresses joint elements modeling the contact plane between the foundation base and the ground surface. The inclusion of these constitutive equations enhances the analytical framework, providing a more accurate representation of the complex interactions involved in determining the UBC and assessing failure mechanisms in eccentrically loaded shallow foundations.

Additionally, the study extensively investigated the effect of the frictional strength ϕ_{soil} of the sandy soil on normalized vertical load V/V_{ult} for rough and smooth foundations. Where, V_{ult} is defined as the UBC of a centric vertical loaded foundation on horizontal sandy soil. The results obtained through RPFEM have provided valuable insights into how these parameters influence the UBC.

2. Methodology for analyzing ultimate bearing capacity

2.1. Constitutive equation for solid elements employing rigid plastic behavior

Tamura et al. [7] derived a rigid plastic constitutive equation for materials with friction, and this investigation utilizes the formulated rigid plastic constitutive equation. The Drucker-Prager yield function is expressed as follows:

$$f(\boldsymbol{\sigma}) = aI_1 + \sqrt{J_2} - b = 0 \quad (1)$$

Where, I_1 represents the first invariant of stress σ_{ij} , with $I_1 = tr(\sigma_{ij})$ where the extension stress is considered positive. J_2 is the second invariant of deviator stress s_{ij} , defined as

$$J_2 = \frac{1}{2} s_{ij} s_{ij}. \text{ Coefficients } a \text{ and } b \text{ denote material constants}$$

associated with the shear resistance angle and cohesion, respectively, under the plane strain condition. The strain rate $\dot{\epsilon}$, characterized as a purely plastic component, must adhere to the volumetric constraint condition governing the soil's dilation property, expressed as:

$$h(\dot{\boldsymbol{\varepsilon}}) = \dot{\varepsilon}_v - \frac{3a}{\sqrt{3a^2 + 0.5}} \dot{\varepsilon} = \dot{\varepsilon}_v - \eta \dot{\varepsilon} = 0 \quad (2)$$

Where, $\dot{\varepsilon}_v$ and $\dot{\varepsilon}$ represent the volumetric strain rate and the norm of the strain rate, respectively. The parameter η is defined in Eq. (2). The stress vector is characterized by two component stresses. The first stress, $\boldsymbol{\sigma}^{(1)}$, uniquely governs the yield function, represents the stress parameter ζ , while the second stress, $\boldsymbol{\sigma}^{(2)}$, represents the indeterminate stress parameter λ . The value of λ remains unknown until the boundary value problem presented in Eq. (2) is resolved.

$$\boldsymbol{\sigma}^{(1)} = \zeta \frac{\partial f}{\partial \boldsymbol{\sigma}} = \frac{b}{\sqrt{3a^2 + 0.5}} \dot{\boldsymbol{\varepsilon}} \quad (3)$$

$$\boldsymbol{\sigma}^{(2)} = \lambda \frac{\partial h}{\partial \dot{\boldsymbol{\varepsilon}}} = \lambda \left(\mathbf{I} - \frac{3a}{\sqrt{3a^2 + 0.5}} \frac{\dot{\boldsymbol{\varepsilon}}}{\dot{\varepsilon}} \right) \quad (4)$$

The Lagrangian method, as formulated by Tamura [8], is employed to express the rigid plastic constitutive equation, and it is given as follows:

$$\boldsymbol{\sigma} = \boldsymbol{\sigma}^{(1)} + \boldsymbol{\sigma}^{(2)} = \frac{b}{\sqrt{3a^2 + 0.5}} \frac{\dot{\boldsymbol{\varepsilon}}}{\dot{\varepsilon}} + \lambda \left(\mathbf{I} - \frac{3a}{\sqrt{3a^2 + 0.5}} \frac{\dot{\boldsymbol{\varepsilon}}}{\dot{\varepsilon}} \right) \quad (5)$$

Hoshina et al. [15], Nguyen et al. [16], and Pham et al. [17] derived the constitutive equation by directly incorporating the constraint condition on the strain rate into the equation, utilizing the penalty method. The stress-strain rate relation for the Drucker-Prager yield function is expressed as follows:

$$\boldsymbol{\sigma} = \frac{b}{\sqrt{3a^2 + 0.5}} \frac{\dot{\boldsymbol{\varepsilon}}}{\dot{\varepsilon}} + \kappa (\dot{\varepsilon}_v - \eta \dot{\varepsilon}) \left(\mathbf{I} - \frac{3a}{\sqrt{3a^2 + 0.5}} \frac{\dot{\boldsymbol{\varepsilon}}}{\dot{\varepsilon}} \right) \quad (6)$$

In this formulation, where κ is a penalty constant and \mathbf{I} is the unit tensor, the Finite Element Method (FEM) coupled with this constitutive equation enables an equivalent analysis of the upper bound theorem for plasticity, termed RPFEM in this study. A notable feature of this constitutive equation is the explicit specification of the relationship between stress and strain rate. Its simplicity and effectiveness in evaluating the limit state of the ground stem from the advantageous omission of an uncertain elastic modulus for the ground. Further details regarding the treatment of the constitutive equation in the rigid body can be found in Hoshina et al. [15].

2.2. Constitutive equation for joint elements employing rigid plastic behavior

At the contact plane, characterized by a discontinuity in displacement velocity, the stress at the limit state is described by the following Coulomb yield function:

$$f(\mathbf{t}) = |t_s| - c_s + t_n \tan \phi_s = 0 \quad (7)$$

where, t_s and t_n represent the shear and normal components of the stress vector at the contact plane, respectively. ϕ_s and c_s are material parameters associated with the frictional strength and cohesive strength at the contact plane.

In this analysis, a zero-thickness joint element is

introduced at the contact plane between two bodies, as illustrated in Fig. 1(a). $\Delta \dot{\mathbf{u}}$ represents the vector of relative displacement velocity along the discontinuous line, $\Delta \dot{\mathbf{u}} = \dot{\mathbf{u}}^+ - \dot{\mathbf{u}}^-$ is depicted in Fig. 1(b). In this study, the joint elements are set into the contact plane between the foundation-soil system in two cases of sandy soil, and sandy soil slope.

The expression for the volumetric constraint condition associated with the Coulomb yield function is as follows:

$$h(\Delta \dot{\mathbf{u}}) = |\Delta \dot{u}_s| \tan \phi_s - \Delta \dot{u}_n \quad (8)$$

$$= \left(\Delta \dot{u}_s \cdot \frac{\tan \phi_s}{|\Delta \dot{u}_s|} - 1 \right) \left(\frac{\Delta \dot{u}_s}{\Delta \dot{u}_n} \right) = \mathbf{a} \cdot \Delta \dot{\mathbf{u}} = 0$$

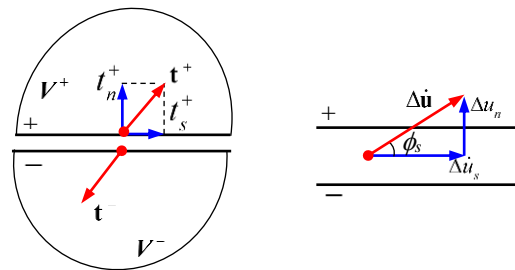
Where, $\Delta \dot{u}_n$ represents a component of the relative displacement velocity normal to the discontinuous line, and $\Delta \dot{u}_s$ is a tangential component. The stress vector is decomposed into the stress component, $\mathbf{t}^{(1)}$, which determines the yield function, and the indeterminate stress component, $\mathbf{t}^{(2)}$, similar to the treatment in the volumetric constraint condition of the solid element. The ensuing equation is derived for the joint element:

$$\mathbf{t}^{(1)} = \gamma_s \frac{\partial f}{\partial \mathbf{t}} = \frac{c_s}{\cos \phi_s (1 + \tan^2 \phi_s)} \frac{\Delta \dot{\mathbf{u}}}{\|\Delta \dot{\mathbf{u}}\|} \quad (9)$$

$$\mathbf{t}^{(2)} = \omega_s \frac{\partial h}{\partial \Delta \dot{\mathbf{u}}} = \omega_s \mathbf{a} \quad (10)$$

where, ω_s is the indeterminate stress parameter, which is ascertained by solving the boundary value problem using Eq. (8) while directly incorporating the volumetric constraint condition with a penalty constant, P . The stress and relative displacement velocity relation for the interface element is expressed as follows:

$$\mathbf{t} = \mathbf{t}^{(1)} + \mathbf{t}^{(2)} = \frac{c_s}{\cos \phi_s (1 + \tan^2 \phi_s)} \frac{\Delta \dot{\mathbf{u}}}{\|\Delta \dot{\mathbf{u}}\|} + P(\mathbf{a} \cdot \Delta \dot{\mathbf{u}}) \mathbf{a} \quad (11)$$



a) stress state on the discontinuity line. b) motion of the discontinuity line
Figure 1. Vector of stress and velocity of relative displacement

3. Effect of foundation roughness on ultimate bearing capacity of shallow foundation on horizontal sandy soil

3.1. Problem definition for horizontal sandy soil

In practice, shallow foundations are commonly employed to support eccentric vertical loads, as observed by researchers such as [18 - 20]. Figure 1 illustrates the sign convention for a shallow foundation subjected to an eccentric vertical load, where e represents the distance from the loading position to the center of the foundation. The dimensions of the model are set to be sufficiently large

to ensure that the boundaries do not influence the failure mechanism and the computed results of the entire system.

The shallow foundation and the sandy soil material are both modeled as rigid plastic materials, with a unit weight of the foundation-soil system denoted as $\gamma_f = \gamma_{soil} = 18 \text{ kN/m}^3$. The cohesion of the shallow foundation is given as $c_f = 500.000 \text{ kPa}$, and the frictional strength of the shallow foundation is specified as $\phi_f = 0 \text{ deg}$. The foundation surface was assumed to be perfectly rough, with the frictional strength and cohesion of the joint elements taken as equal to that of the sandy soil ($\phi_s = \phi_{soil}$, and $c_s = c_{soil}$). Meanwhile, the properties of the smooth surface were considered as $\phi_s = 0$ and $c_s = 0$. In natural, the frictional strength of sandy soil can vary within values of 30deg, 35deg, and 40deg. The key factor for determining the properties of the joint elements is based on the properties of the sandy soil. Using the joint element to simulate the contact surface between the foundation and the ground involves employing 200 nodes and 100 joint elements. These elements facilitate the modeling of the interface, allowing for an accurate representation of the interaction between the footing and the underlying soil. This approach enhances the structural analysis by considering the complex behavior at the contact points and provides a more realistic simulation of the foundation-ground interaction. The study encompasses both rough and smooth foundations, as shown in Table 1. In the computation process, a concentrated load was applied at nodes of the shallow foundation to define the prescribed load and the load coefficient. The ultimate bearing capacity was assessed by computing the limit value for this load coefficient.

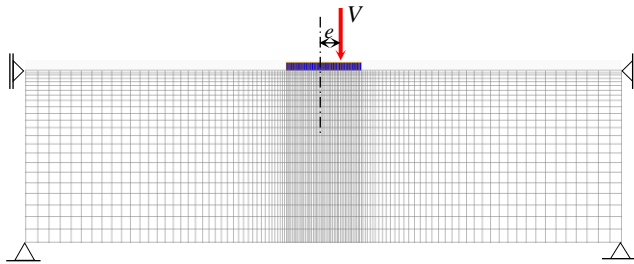


Figure 2. Sign convention of a shallow foundation against eccentric vertical load on horizontal sandy soil

Table 1. Parameters for foundation roughness

Parameter	Rough foundation	Smooth foundation
Frictional strength ϕ_s (deg)	30, 35, 40	0
Cohesion c_s (kPa)	0	0

For an eccentric vertical load, Figure 3 illustrates the distribution of contact normal stress ($\sigma_n/\gamma B$) along the foundation corresponding to the distance X , where X represents the location in the foundation relative to the center of the foundation base. The normal contact stress $\sigma_n/\gamma B$ is computed based on the interaction force of the nodes at the joint elements. For the smooth foundation, the shear stress component is equal to $\tau/\gamma B = 0$, while for the rough foundation, the shear stress component is $\tau/\gamma B \neq 0$. It is evident that the size of the $\sigma_n/\gamma B$ distribution decreases rapidly as the eccentric length e increases, regardless of the foundation roughness. Additionally, the maximum contact

stress ($\sigma_n/\gamma B$) for the rough foundation is observed to be higher than that for the smooth foundation. This phenomenon arises from the observation that the ultimate bearing capacity (UBC) of a rough foundation surpasses that of a smooth foundation. This substantiates the substantial impact of foundation roughness on the distribution of normal stress. When $e=0.0B$, the maximum value of σ_n is generally close to $-11.10\gamma B$ for the rough foundation and $-8.81\gamma B$ for the smooth foundation. However, for $e \geq 0.1B$, a zero-contact stress zone ($\sigma_n/\gamma B = 0$) is observed along the left side of the foundation edge. This occurs because there is no interaction force transmitted from the foundation base to the ground surface in this region. This zone with $\sigma_n/\gamma B = 0$ signifies the detachment zone of the foundation-soil system. The study has clarified the effects of foundation surface roughness and eccentricity e on normal contact stress.

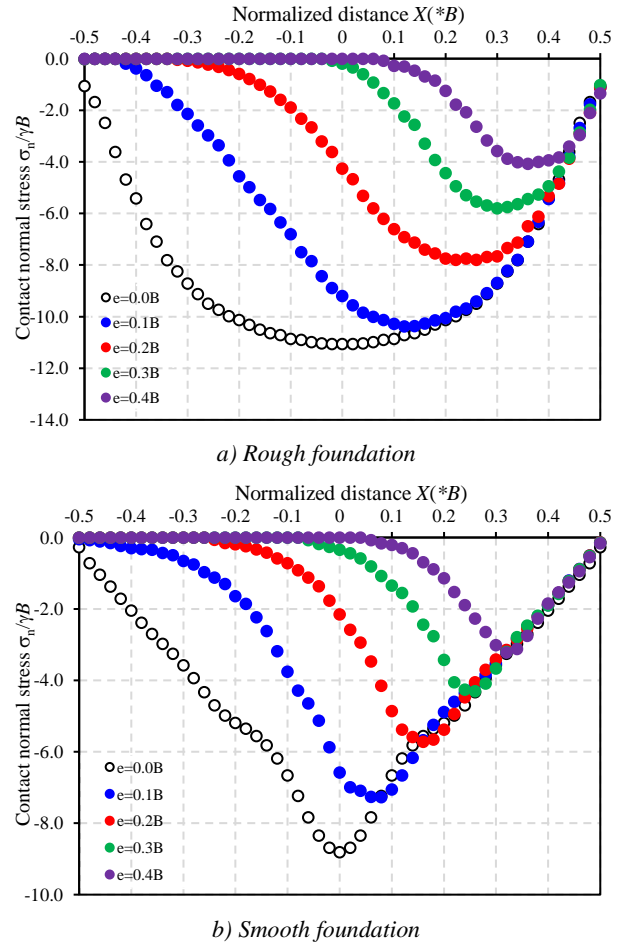


Figure 3. Distribution of contact normal stress $\sigma_n/\gamma B$ along foundation base on horizontal sandy soil of $\phi_{soil} = 30 \text{ deg}$

3.2. Effect of foundation roughness on V/V_{ult} ratio

For an eccentric vertical load, Figure 4 illustrates the effect of foundation roughness on the normalized vertical load (V/V_{ult}) for different frictional strengths of the sandy soil ($\phi_{soil} = 30 \text{ deg}$, 35 deg , and 40 deg), where V_{ult} represents the ultimate bearing capacity computed for the centric vertical load. The properties of the joint elements for the rough and smooth foundations are outlined in Table 1. It is evident that the V/V_{ult} ratio decreases proportionally as the normalized eccentricity (e/B) increases. However, the

trend in the decrease of the V/V_{ult} ratio is independent of both the value of ϕ and the foundation roughness. These results align well with the solution of Meyerhof [1].

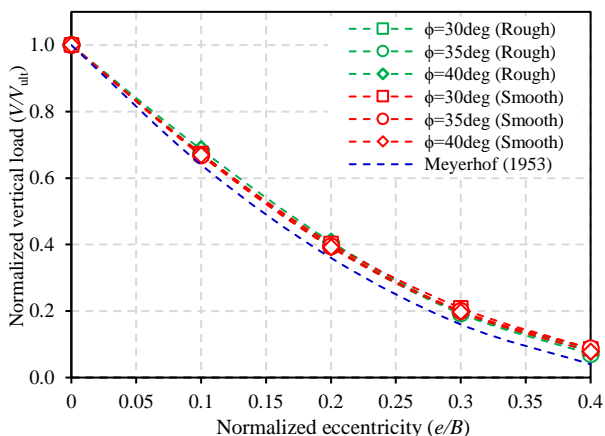
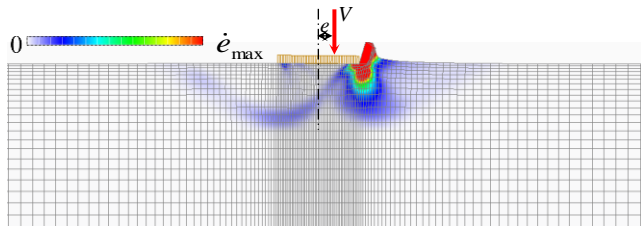
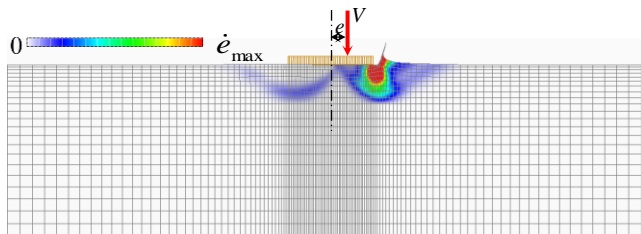


Figure 4. Effect of foundation roughness on normalized vertical load (V/V_{ult}) for various value of ϕ_{soil}

Figure 5 shows the deformation diagram of a shallow foundation with an eccentric length of $e=0.1B$ for rough and smooth foundations. It is apparent that the failure area for the rough foundation is deeper than that for the smooth foundation. The failure mechanisms of the foundation-soil system are divided into two different zones and align well with the solutions presented by [2, 4]. The ultimate bearing capacity was computed to be approximately $V=2584$ kN/m for the rough foundation and $V=1334$ kN/m for the smooth foundation, which is 52% of the rough foundation. The study has clarified the effects of foundation surface roughness and eccentricity e on the failure mechanism of strip foundation on horizontal sandy soil.



a) $e=0.1B$ ($V=2584$ kN/m) for rough foundation



b) $e=0.1B$ ($V=1334$ kN/m) for smooth foundation

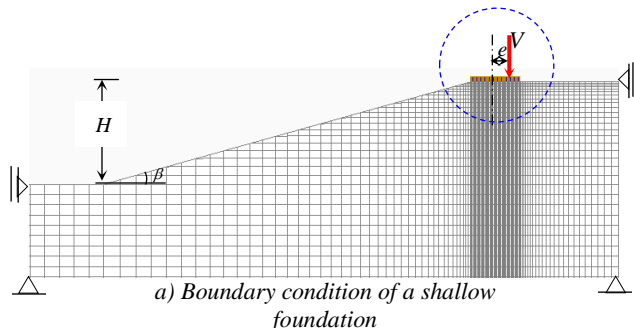
Figure 5. Deformation diagram of a shallow foundation on horizontal sandy soil of $\phi_{soil}=30$ deg under eccentric load

4. Effect of foundation roughness on ultimate bearing capacity of shallow foundation on sandy soil slope.

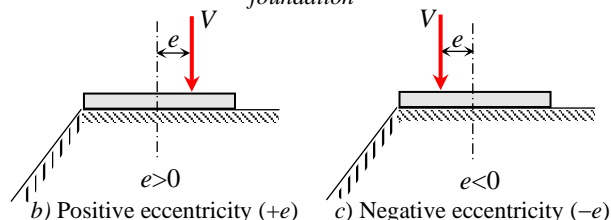
4.1. Problem definition for sandy soil slope

By the asymmetry of the foundation-soil system, the study focuses on the effect of eccentric direction on the ultimate bearing capacity and the failure mechanism of a

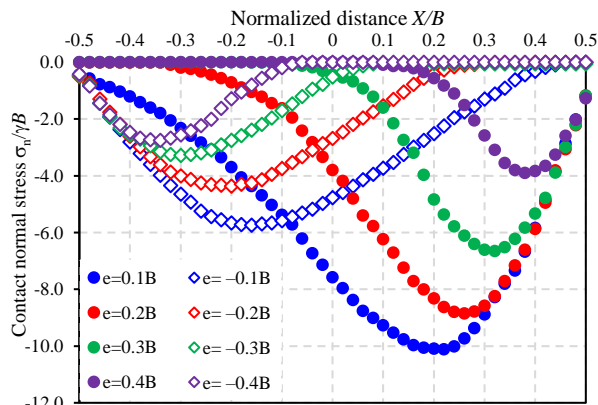
shallow foundation on crest sand slope. The slope geometry is defined by slope angle β , slope height H . A new sign convention has been used to define positive eccentricity and negative eccentricity, as shown in Figure 6. Positive eccentric direction e is defined as the loading point on the right side of the shallow foundation. While negative eccentric direction e is defined as the loading point on the left side of the foundation towards the slope.



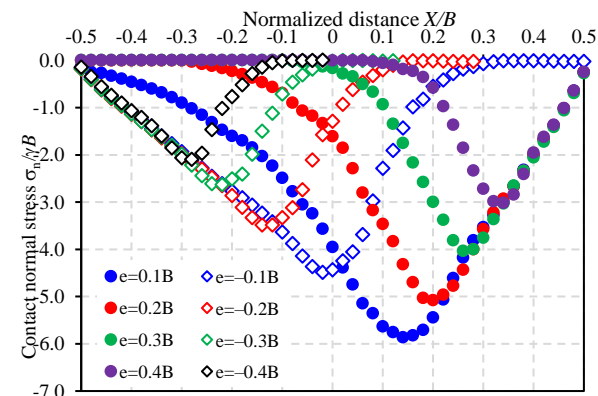
a) Boundary condition of a shallow foundation



b) Positive eccentricity (+e) c) Negative eccentricity (-e)
Figure 6. Sign convention of a shallow foundation against eccentric vertical load placed on crest sand slope.



a) Rough foundation



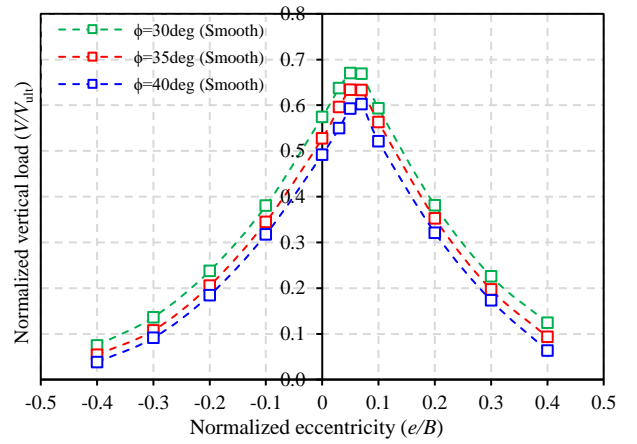
b) Smooth foundation

Figure 7. Distribution of contact normal stress $\sigma_n/\gamma B$ at foundation base on sandy soil slope of $\phi_{soil}=30$ deg with slope geometry of $\beta=15^\circ$, $H=2.0B$, and $L=0.0B$

A comprehensive analysis was conducted for a typical case of the crest of a sandy soil slope with $\phi_{\text{soil}}=30\text{deg}$, a slope angle $\beta=15^\circ$, and a slope height $H=2.0B$. The distribution of normal contact stress ($\sigma_n/\gamma B$) acting on the foundation base was studied for two different foundation roughness conditions, as shown in Figure 7. The figure demonstrates that the normal contact stress for the positive eccentric direction was found to be significantly larger than that for the negative eccentric direction, regardless of the different foundation roughness. The maximum value of normal stress for a rough foundation is observed to be higher than that for a smooth foundation. For a positive eccentricity of $e=0.1B$, the maximum value of σ_n is $-10.1\gamma B$ for the rough foundation, while it is $-5.87\gamma B$ for the smooth foundation. For a negative eccentricity of $e=-0.1B$, the maximum value of σ_n is $-5.66\gamma B$ for the rough foundation, while it is $-4.49\gamma B$ for the smooth foundation. As the eccentric length e increases, the size of the normal stress distribution decreases. This is because the UBC of the foundation-soil system decreases rapidly with an increasing eccentricity e . The eccentric direction has a significant effect on the distribution of normal contact stress for both rough and smooth foundations.

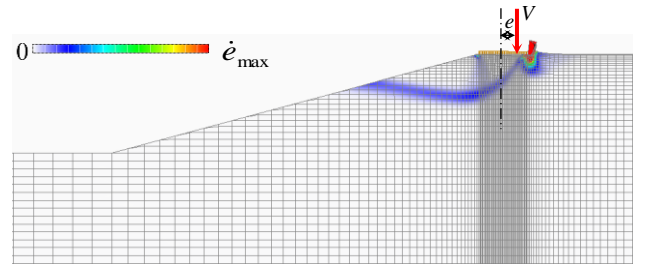
4.2. Effect of foundation roughness on V/V_{ult} ratio

For an eccentric vertical load, Figure 8 indicates the influence of foundation roughness on the normalized vertical load (V/V_{ult}) for various ϕ_{soil} values (30deg, 35deg, and 40deg) under typical conditions of $\beta=15^\circ$ and $H=2.0B$. The findings show a significant effect of both the frictional strength ϕ_{soil} and foundation roughness on the V/V_{ult} ratio. As the frictional strength ϕ_{soil} increases, the maximum V/V_{ult} values decrease. This contrasts with the results observed in horizontal sandy soil, where the V/V_{ult} ratio remained unaffected by both frictional strength ϕ_{soil} and foundation roughness. Notably, the maximum V/V_{ult} value for a smooth foundation is observed to be higher than that of a rough foundation. This discrepancy arises due to the slip surface of the shallow foundation reaching the slope surface in the foundation-soil system, leading to a rapid decrease in ultimate bearing capacity (UBC). The outcomes obtained from the RPFEM offer a clear insight into how foundation roughness and frictional strength ϕ_{soil} collectively influence the V/V_{ult} ratio.

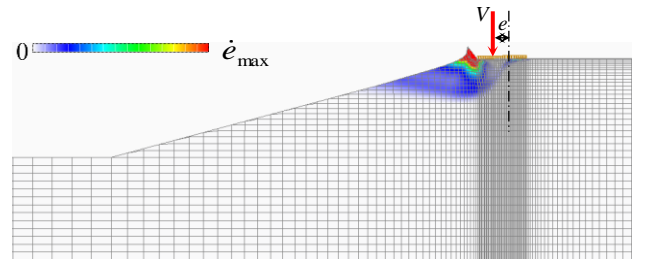


b) Smooth foundation

Figure 8. Effect of foundation roughness on normalized vertical load (V/V_{ult}) for various value of ϕ_{soil} with slope geometry of $\beta=15^\circ$, $H=2.0B$, and $L=0.0B$



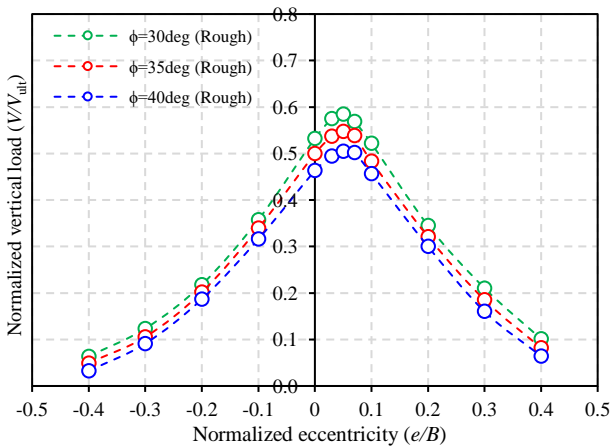
a) Positive eccentricity $e=0.1B$ ($V=1909$ kN/m)



b) Negative eccentricity $e=-0.1B$ ($V=1308$ kN/m)

Figure 9. Deformation diagram of a shallow foundation on sandy soil slope of $\phi_{\text{soil}}=30$ deg under eccentric vertical load for rough foundation

Figures 9 and 10 illustrate the failure mechanisms of the foundation-soil system under two different eccentric directions ($e=\pm 0.1B$) for both rough and smooth foundations, respectively. In the case of positive eccentricity ($e=+0.1B$), the failure mechanism exhibits a "both-sided" failure mode, as depicted in Figures 9a and 10a, with the failure domain primarily concentrated on the right-hand side of the foundation. Conversely, for negative eccentricity ($e=-0.1B$), the failure mechanism adopts a "single-sided" mode, as shown in Figures 9b and 10b, with an unsymmetrical rigid wedge observed beneath the shallow foundation base. For the rough foundation, the ultimate bearing capacity (UBC) is determined to be $V=1909$ kN/m for $e=+0.1B$ and $V=1308$ kN/m for $e=-0.1B$, representing 69% of positive eccentricity. As for the smooth foundation, the UBC values are $V=1158$ kN/m for $e=+0.1B$ and $V=743$ kN/m for $e=-0.1B$, indicating 64% of positive eccentricity. These findings demonstrate that the



a) Rough foundation

UBC of the foundation-soil system performs better under positive eccentricity compared to negative eccentricity. The analysis results derived from RPFEM provide valuable insights into the influence of eccentric directions on the failure mechanisms and the UBC of the foundation-soil system for both rough and smooth foundations.

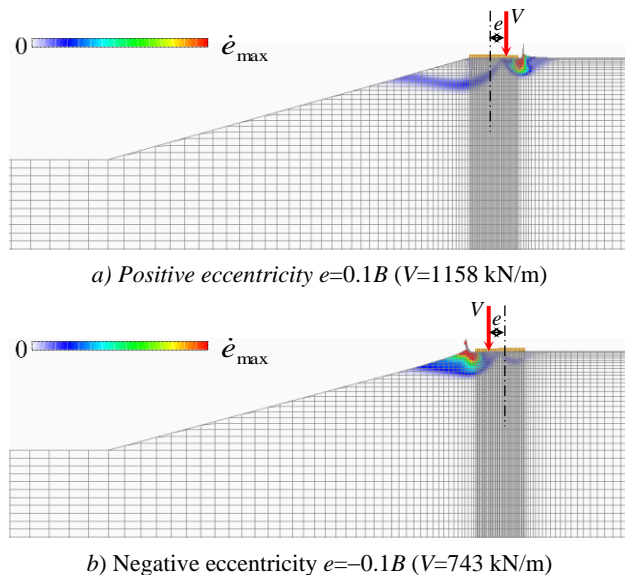


Figure 10. Deformation diagram of a shallow foundation on sandy soil slope of $\phi_{soil}=30$ deg under eccentric vertical load for smooth foundation

5. Conclusions

The key conclusions can be summarized as follows:

(1) Joint element effectiveness: The use of a joint element proved effective in evaluating the ultimate bearing capacity of a shallow foundation under eccentric vertical loads. This element facilitated the calculation of contact normal stress at the foundation-soil interface, revealing the significant impact of foundation surface roughness on failure mechanisms, particularly on horizontal sandy soil and sandy soil slopes.

(2) Influence of foundation roughness and frictional strength: The study extensively investigated the effect of foundation roughness and soil strength on the V/V_{ult} ratio in the cases of horizontal sandy soil and sandy soil slopes. Results from the RPFEM analysis demonstrated that, for horizontal sandy soil, the V/V_{ult} ratio remained unaffected by variations in foundation roughness and frictional strength ϕ . However, a substantial impact was observed in sand slopes, where the slip surface extended to the slope surface, causing a rapid decrease in ultimate bearing capacity compared to horizontal sandy soil.

(3) Influence of eccentric direction: Under positive eccentricity, both rough and smooth foundations exhibited a robust "both-sided" failure mode, showcasing superior ultimate bearing capacity compared to the "single-sided" mode observed under negative eccentricity. This insight, derived from RPFEM analysis, underscores the critical influence of eccentric directions on failure mechanisms and ultimate bearing capacity of foundation-slope system.

Acknowledgment: This work was supported by The University of Danang - University of Science and Technology, code number of Project: B2022-DN02-16.

REFERENCES

- [1] G. Meyerhof, "The bearing capacity of foundations under eccentric and inclined loads", In *Proc. of 3rd ICSMFE*, vol. 1, 1953, pp. 440-445.
- [2] D.T. Loukidis, Chakraborty, and R. Salgado, "Bearing capacity of strip footings on purely frictional soil under eccentric and inclined loads", *Canadian Geotechnical Journal*, vol. 45, no. 6, pp. 768-787, 2008.
- [3] C. Tang, P. Kok-Kwang, and T. Kim-Chuan, "Effect of footing width on N_y and failure envelope of eccentrically and obliquely loaded strip footings on sand", *Canadian Geotechnical Journal*, vol. 52, no. 6, pp.694-707, 2015.
- [4] P. N Quang, S. Ohtsuka, K. Isobe, Y. Fukumoto, and T. Hoshina, "Ultimate bearing capacity of rigid footing under eccentric vertical load", *Soils and Foundations*, Vol. 59, no. 6, pp.1980-1991, 2019.
- [5] P. N. Quang, S. Ohtsuka, K. Isobe, and Y. Fukumoto, "Limit load space of rigid footing under eccentrically inclined load", *Soils and Foundations*, vol. 60, no. 4, pp. 811-824, 2020.
- [6] T. Tamura, K. Shoichi, and S. Tetsuya, "Limit analysis of soil structure by rigid plastic finite element method", *Soils and Foundations*, vol. 24, no. 1, pp. 34-42, 2020.
- [7] T. Tamura, K. Shoichi, and S. Tetsuya, "Rigid-plastic finite element method for frictional materials", *Soils and Foundations*, vol. 27, no. 3, pp. 1-12, 1987.
- [8] T. Tamura, "Rigid-plastic finite element method in geotechnical engineering", In *Computational Plasticity, Current Japanese Material Research*, 1990.
- [9] A. Asaoka and S. Ohtsuka, "The analysis of failure of a normally consolidated clay foundation under embankment loading", *Soils and Foundations*, vol. 26, no. 2, pp. 47-59, 1986.
- [10] A. Asaoka and S. Ohtsuka, "Bearing capacity analysis of a normally consolidated clay foundation", *Soils and foundations*, vol. 27, no. 3, pp. 58-70, 1987.
- [11] A. Asaoka, S. Ohtsuka, and M. Minoru, "Coupling analyses of limiting equilibrium state for normally consolidated and lightly overconsolidated soils", *Soils and Foundations*, vol. 30, no. 3, pp. 109-123, 1990.
- [12] P. N. Quang and S. Ohtsuka, "Ultimate bearing capacity of rigid footing on two-layered soils of sand-clay", *International Journal of Geomechanics*, vol. 21, no. 7, 04021115, 2021.
- [13] P. N. Quang, S. Ohtsuka, K. Isobe, and Y. Fukumoto, "Limit load space of rigid strip footing on cohesive-frictional soil subjected to eccentrically inclined loads", *Computers and Geotechnics*, vol. 151, 104956, 2022.
- [14] P. N. Quang, S. Ohtsuka, K. Isobe, P. N. Vinh, and H. P. Hoa, "Limit load space of rigid strip footing on sand slope subjected to combined eccentric and inclined loading", *Computers and Geotechnics*, vol. 162, 105652, 2023.
- [15] T. Hoshina, "Rigid plastic stability analysis for slope including thin weak layer", *Geotech. J.*, vol. 6, no. 2, pp. 191-200, 2011.
- [16] L. D. Nguyen, S. Ohtsuka, T. Hoshina, and K. Isobe, "Discussion on size effect of footing in ultimate bearing capacity of sandy soil using rigid plastic finite element method", *Soils and foundations*, vol. 56, no. 1, pp. 93-103, 2016.
- [17] P. N. Quang, S. Ohtsuka, K. Isobe, and Y. Fukumoto, "Group effect on ultimate lateral resistance of piles against uniform ground movement", *Soils and Foundations*, vol. 59, no. 1, pp. 27-40, 2019.
- [18] A. Guetari, B. Sadok, and M. S. Remadna, "Effect of the eccentric load on the bearing capacity of a strip footing founded on sand", *Journal of Applied Engineering Science & Technology*, vol. 4, no. 2, pp. 171-176, 2018.
- [19] P.N. Quang and S. Ohtsuka, "Numerical Investigation on Bearing Capacity of Rigid Footing on Sandy Soils Under Eccentrically Inclined Load", In *Proceedings of the 2nd Vietnam Symposium on Advances in Offshore Engineering: Sustainable Energy and Marine Planning*, Springer Singapore, 2022, pp. 333-341,
- [20] P.N. Quang, S. Ohtsuka, K. Isobe, and Y. Fukumoto, "Consideration on Limit Load Space of Footing on Various Soils Under Eccentric Vertical Load", In *Challenges and Innovations in Geomechanics: Proceedings of the 16th International Conference of IACMAG*, volume 126, Springer International Publishing, 2021, pp. 75-84.